Mesoγ-Scale Distribution of Orographic Precipitation: Numerical Study and Comparison with Precipitation Derived from Radar Measurements

PINHAS ALPERT AND HAIM SHAFIR

Department of Geophysics and Planetary Sciences, Tel Aviv University, Tel Aviv, Israel

(Manuscript received April 1988, in final form 6 September 1988)

ABSTRACT

On the assumption that moisture convergence due to mechanical uplifting approximately equals the orographic precipitation, the mesoγ-scale rainfall distributions over mountainous regions in Israel are investigated. The simulated distributions are compared to rainfall observations both from raingages and from radar reflectivities. The mean error in the predicted rainfall on scale of 2 km was ±8.4% for mean annual normals and 15%–20% for three case studies. It is suggested that orographic rainfall on the small mesoscale is highly predictable with the adiabatic assumption that the uplifting is determined by $\mathbf{V} \cdot \nabla Z_s$, where $\mathbf{V}$ is the horizontal wind encountering the mountain and Z_s is the topographic elevation.

It is also illustrated that the climatological observed rainfall distribution could be complemented by the model at locations where sufficient observations were not available. By comparison of the model simulation with the radar-derived rainfall, the considerable effect that a change in the wind direction has on the orographic rainfall distributions is shown.

1. Introduction

One of the most difficult problems in mountain meteorology is the accurate prediction of precipitation over complex topography. This is important for weather prediction, but particularly in hydrological and agricultural applications.

The characteristics of orographic rain and favorable conditions for heavy rainfall in southern England were reviewed by Browning (1980). The seeder–feeder mechanism suggested by Bergeron (1965) was accepted as a reasonable explanation for mesoscale orographic rain. Theoretical studies by Collier (1975), Storebo (1976), Bader and Roach (1977), Bell (1978), Richard et al. (1987) and others supported this idea, but these models, as well as others over complex topography, have not compared the mesoγ ($\Delta x \sim 2$ km) precipitation in two horizontal directions with a similar resolution in the observations. Not only are there difficulties of applying a refined three-dimensional mesoγ model, but there is also the problem that high-resolution precipitation data over complex terrain is generally unavailable. Closer to current approach is the study by Rhea (1978), who applied a two-dimensional, steady state orographic precipitation model over topography. Rhea (1978) took into account moisture depletion by upstream barriers but applied his model to a coarser grid ($\Delta x = 10$ km) and have compared the model results with mainly integrated raingage data for primarily hydrological uses.

Hill et al. (1981; hereafter called HBB) and consequently Collier and Knowles (1986) have shown that radar data over complex topography could be carefully used for estimating the mesoscale distribution of precipitation over mountains in southern Wales and northwest England. They compared the radar data with raingage observations and studied the structure and mechanisms of orographic rain. One of the important results of HBB was that low-level wind speed strongly influences the orographic enhancement. Alpert (1986) has shown that the orographic rain enhancement over two-dimensional cross sections of high mountains could be well estimated by the assumption that the moisture convergence due to the horizontal wind vector encountering the mountain slope is proportional to the rain enhancement.

In the present study, we extend the formula suggested by Alpert (1986) to a horizontal two-dimensional plane that follows the terrain and investigate the applicability of the method over a lower mountainous region in Israel. In particular, predicted distributions of precipitation over the Judean Mountains (400 to 800 m elevations) are compared to observed distributions as derived from radar measurements by Rosenfeld (1986) as well as to raingage data. This is performed for three case studies (see sections 5, 6) and for the average annual rainfall (see section 4). Sections 2 and 3 briefly describe the model and some numerical aspects.

Corresponding author address: Dr. Pinhas Alpert, Dept. of Geophysics and Planetary Sciences, Tel Aviv University, Ramat Aviv, 69978, Tel Aviv, Israel.

2. The model

The precipitation at a point (x, y) whose altitude is given by $Z_s(x, y)$ is estimated by

$$P \approx \rho q(\mathbf{V} \cdot \nabla Z_s + W_l) + E, \quad (1)$$

where P and E represent precipitation rate and evaporation, ρ, q and $\mathbf{V}$ are mean air density, mean specific humidity and mean horizontal velocity in the planetary boundary layer, respectively, and W_l is the large scale (synoptic) vertical velocity contribution. Similar expressions were used to estimate tropical precipitation, e.g., Holton (1979, p. 342) and Stevens and Lindzen (1978), except we added the topographical contribution, $\mathbf{V} \cdot \nabla Z_s$, to the vertical velocity at the top of the moist boundary layer. In the present formulation a constant depth of the converging boundary layer is assumed, to follow the topography. In the forthcoming experiments it was taken as 1000–900 mb above MSL or about 1 km over the topography. The W_l is deduced from precipitation P_0 at an upstream location at mean sea-level height; see Alpert [1986, Eq. (32)]. Basically, the precipitation is determined by the uplift induced by the wind vector encountering the local slope and the decrease of moisture availability, ρq, with topographic height. Over mountains, the evaporation contribution was shown to be small when the relative humidity is relatively large (>85%) and (1) could be rewritten as

$$P = \epsilon r e_s(Z_s)[\mathbf{V} \cdot \nabla Z_s + W_l]/[RT(Z_s)], \quad (2)$$

where $\epsilon = 0.622$, $r = e_a/e_s$ (e_a and e_s are the air vapor pressure and the saturated surface vapor pressure), R is the gas constant, and $T(Z_s)$ the temperature at the altitude Z_s is assumed to decrease with elevation by a constant moist adiabatic lapse rate Γ.

Equation (2) represents (excluding W_l) the net contribution to the precipitation induced by the local topographical uplifting only where the other mountain effects on the dynamical flow as well as microphysical processes are ignored. For comparison with observations, it was shown to be useful to advect the precipitation downstream by the horizontal wind $\mathbf{V}$. Accordingly the precipitation became the normally weighted sum of the values upstream. The Gaussian weight function W_i was chosen with a standard deviation (σ) proportional to the advective velocity $|\mathbf{V}|$ multiplied by the lifetime scale of the precipitating cloud (t). Following Alpert (1986, formula 33), the precipitation P_0 at any point 0 is recalculated by

$$P_0 = \frac{1}{W} \sum_{i=0}^{N} W_i P_i,$$

where

$$W = \sum_{i=0}^{N} W_i$$

$$W_i = \exp[-(x_i - x_0)^2/2\sigma^2]$$

$$\sigma = |\mathbf{V}| \cdot t. \quad (3)$$

For N we have found that 5 was sufficient for the following experiments. According to (3) the precipitation P_0 is determined by the sum of the weighted precipitations upstream. All rainfall results thus obtained were multiplied by a constant efficiency factor. This factor represents precipitation efficiency as discussed by Alpert (1986) and serves as a tuning parameter in the model simulations; see also section 7e.

The wind vector of the 1000–900 mb layer was employed to represent the mean boundary-layer velocity in the following experiments.

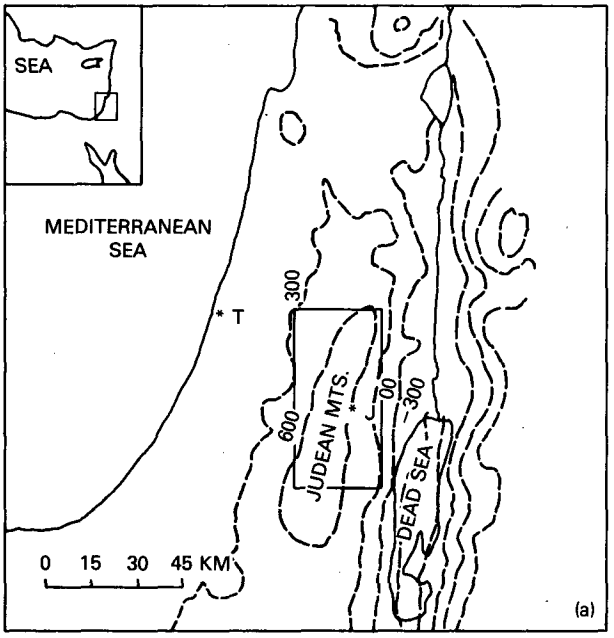

FIG. 1a. General location of the study domain. Topographic contours are with 300 m intervals. Rectangular area denotes the model domain. Letters T and J stand for towns of Tel Aviv and Jerusalem, Israel.

3. Topography and some numerical aspects

The study domain was a 30 × 60 km rectangle over the Judean Mountains located in central Israel (Fig. 1a) using a grid interval of $\Delta x = \Delta y = 2$ km. Rainfall averages for the winter rain season exceed 700 mm while upstream, along the coast, values range from 400 to 500 mm; e.g., see Wolfson (1975). The rainfall enhancement over the mountains is particularly high later in the winter as the coastal contribution diminishes and the mountainous rainfall may even become double or more than double the corresponding amounts on the coast (two to five times more in the forthcoming case study of February 1983).

The study domain is shown in Fig. 1b. Elevations exceeding 800 m are shaded, and locations of raingages employed in this study are denoted. In the following experiments, (2) was solved numerically over the grid covering this domain,[1] where first the input parameters for average rain conditions were applied to be compared with annual normals (section 4). This is followed (section 5) by a simulation for a specific case on 18 February 1983 where the rain was expected to be strongly orographic. Two additional cases with relatively large amounts of orographic rain are described in sections 5–6: one in early winter (31 December 1982) and the other on 4 March 1983, but with a southwesterly wind.

4. Simulated and observed annual rainfall averages

Input values were obtained from upstream radiosondes at Bet-Dagan (located at the radar site near point T, see Fig. 1a) typical for rain situations in the Judean Mountains: temperature lapse rate, $\Gamma = 6.5°C\ km^{-1}$; sea-level surface temperature, $T_0 = 291$ K; $\mathbf{V} = 270°/10\ m\ s^{-1}$ and upstream sea-level site rainfall rate, $P_0 = 550\ mm\ yr^{-1}$. Upstream relative humidity varies from 70% in the south to 100% in the north based on the radiosonde and surface observations upstream. Relative humidities also drop linearly by 15% from west to east. Table 1 lists the input parameters for the present and subsequent experiments presented in this study.

The model-simulated and observed average annual rainfall rates are shown in Figs. 2a and 2b. The observations are based upon about 58 gages for the period from 1931 to 1960. Results indicate the basic features of the observed distribution as for example, the location of the 700 mm yr^{-1} maximum on a rainfall ridge from the north toward the southwest. Notice also the 600 mm yr^{-1} contour southwest to Bethlehem (i.e., BL) which extends to the southwesterly direction and the minimum of 500 mm yr^{-1} to its westerly side. In general, many smaller-scale features appear in the model but do not exist in the observations. The most prominent of these is probably the 700 mm maximum at coordinates (693, 513) (see Fig. 2a, far to the west of BL). Not only does this maximum not appear in Fig. 2b—derived from observations—but it seems to be a region of a minimum. A closer look at the reporting stations at this site (Fig. 1b), reveals that this area farther to the west of BL does not contain any stations. Presumably, this fact explains the apparent contradiction between the model and the observations. It also exemplifies how the model and observations could be complementary to each other. In this case it strongly suggests substituting the relative minimum west of BL (in the observation-derived distribution, Fig. 2b) by the maximum of about 700 mm yr^{-1} predicted by the model.

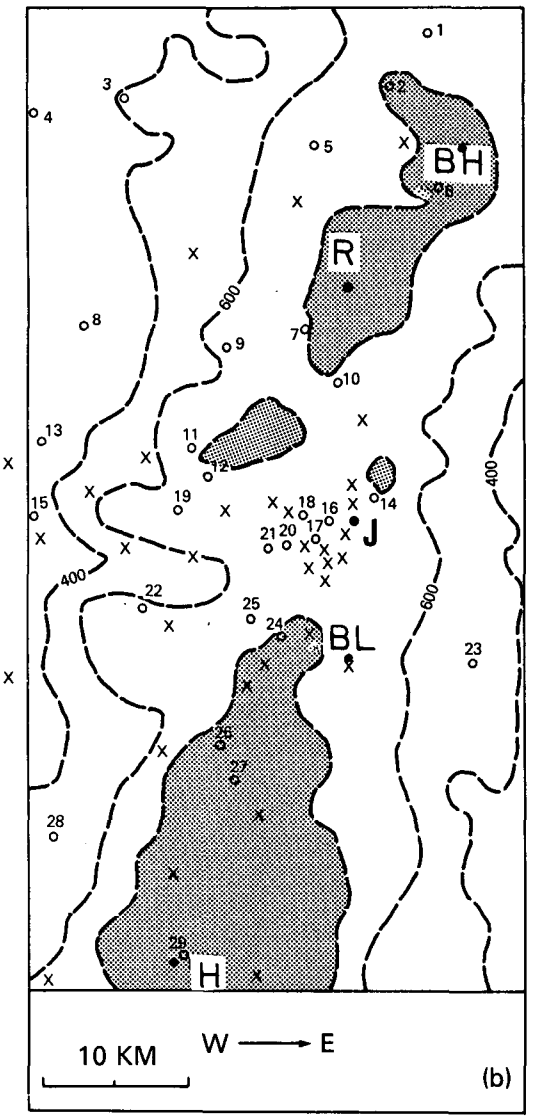

FIG. 1b. Study domain. Topographic contours are with 200 m intervals. Shaded region is higher than 800 m. The circles and crosses denote gages that are used later. Twenty-nine circled stations were used in the case studies. The crossed gages were used only for the annual averages. Locations R, BH, J, BL and H stand for Ramalla, Baal-Hatsor, Jerusalem, Bethlehem, and Hebron.

The correlation between the modeled and observed average annual rainfall for all of the rainfall gage data is presented in Fig. 3. From about 58 stations, only 6 had errors larger than 20% and the coefficient of correlation is 0.67 (it increases to 0.74 when the two circled stations are omitted); see Table 2. This correlation seems very reasonable considering the highly simplified model and that we did not smooth the height of the

[1] In the numerical computation five additional points have been added upstream to allow realistic advection. Hence, the full numerical domain starts at the coordinate 680 (east) and 480 (north); e.g., see Fig. 2a.

TABLE 1. Input parameters for the model for the various experiments.

No.	Experiment date	Rain period/ Rainfall efficiency	Wind (deg/m s^{-1})	Upstream precipitation P_0 (mm)	MSL temperature T_0 (K)	Lapse rate (°C/km)	Relative humidity variation upstream (%)		RH at MSL (%) (northwest corner)
							Horizontal (y-north)	Vertical (z-upward)	
1.	Annual	47 d*/0.1	270/10	550	291	6.5	+30 (also −15 in the x-direction)**	0	100
2.	18 Feb 1983	24 h/0.5	270/21	18	280.5	6.5	+12	0	100
3.	31 Dec 1982–2 Jan 1983	3 d/0.33	270/14	50	283	7.0	+19	+7	80
4.	4 Mar 1983	24 h/0.75	240/16.5	20	285	7.0	+20	+6	92

* Based on average annual number of rainfall days in the area.
** For the annual normals the decrease of moisture availability towards the east was also incorporated.

raingage site over an area surrounding the point (e.g., see Hill et al. 1981). We have obtained similar results over the high Galilee mountains for an area of 30 × 20 km and the correlation coefficients there for 22 stations was found to be 0.80. To achieve better resolution in observations that will enable us to estimate the model performance and consider the smaller scale features of the rainfall distribution, the rainfall as derived from radar over the same region will be employed in the next two sections.

5. Simulated and radar-derived rainfall distribution—18 February 1983

The radar site is Bet-Dagan at about 20 to 60 km from the study domain. The radar had a wavelength of 5.6 cm, a 1.6° conical beam, and an antenna tilt of 0.8°. The calibration of the Z–R relationship was based only upon stations to the west of the clutter regions (west of the study domain). The radar-derived rainfall amounts are therefore underestimated not only due to the distance and the mountains, but also by the calibration. On 18 February 1983, rainfall amounts in the study area reached 50 mm while, at the coastal regions, rainfall amounts were typically 10 to 20 mm. The integrated rainfall was derived from the radar by Rosenfeld (1986). The permanent ground clutter and the topography in the study region are shown in Fig. 4. It should be pointed out that the ground clutter for different days for the same winter were overlapped to remove any point suspicious for false results.

The input parameters for this case[2] were as follows: P_0 = 18 mm d^{-1}; V = 270°/21 m s^{-1}; T_0 = 280.5 K; Γ = 6.5°C km^{-1}. The upstream surface relative humidities vary from 88% in the south to 100% in the north based on the reports upstream; see Table 1.

The synoptic configuration on the 18 February 1983 was that of a "Cyprus low" with strong cold westerly flow over the southeastern Mediterranean. A minimum surface pressure of 989 mb was reported over southeastern Turkey while at Lod, Israel, 1003 mb was recorded on 18 February. Although the low gradually weakened from the 18th for the next 48 hours, it remained almost stationary in southeastern Turkey and the cyclonic pressure gradient over the eastern Mediterranean—including the study area over the Judean Mountains—stayed very pronounced with no appreciable weakening until the 21st when the low reorganized over the Caspian Sea. The lower troposphere over Israel was typified by a thoroughly saturated layer from the surface to about 600 mb (~4 km) and relatively very cold air at the upper level, i.e., −28°C at 500 mb and −2°C at 850 mb.

[2] It should be noted that the input values given in Table 1 correspond to the model runs to be compared with the radar-derived results. In the model runs compared with the raingage observations, slightly different input parameters were employed, because the integration periods did not exactly overlap.

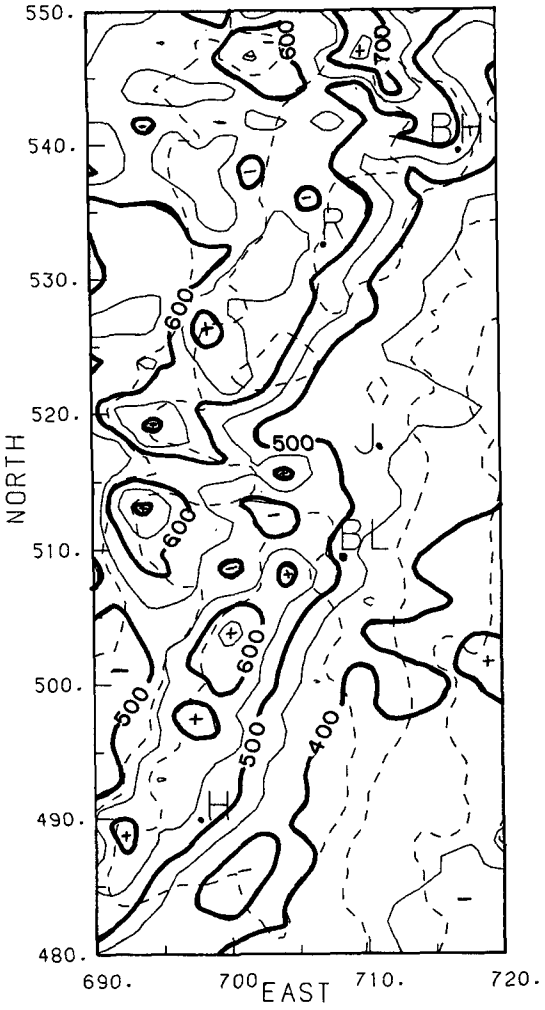

FIG. 2a. Contours of average annual rainfall from the model. Dashed lines are topographic contours as in Fig. 1b. Grid numbers are in kilometers; rainfall contour interval of 50 mm yr^{-1}.

Figures 5a and 5b present the model- and radar-integrated 24-h rainfall starting at 0600 UTC 18 February 1982. Clutter regions are depicted in both maps so that comparison in the relevant region could be performed. As mentioned earlier, rainfall results are largely underestimated both in the radar-derived rainfall and in the model. For example, gages 10 and 16 (see Fig. 1b) collected 46.0 and 39.5 mm, while radar-derived values were 17.7 and 10.3 mm and model values were 27 and 21 mm, respectively. Although absolute values are much smaller in Figs. 5a and 5b, the relative values are those of primary interest here. Both patterns are remarkably similar in many of their small-scale features. Maxima and minima as well as ridges and troughs are indicated by + and −, respectively. In particular, notice the outstanding rainfall trough from Jerusalem extending to the west-northwest which appears in both the model and the observations. In the model, however, this trough is slightly rotated to the west (anticlockwise sense) compared to the observed trough.

A similar trough exists also in the north extending from the station Baal-Hatsor (BH) towards the northwest. Also, the maximum at (693, 513) discussed earlier with regard to the annual normals reappears in this simulation not only is the model, but even more interestingly in the radar-derived rainfall; see Fig. 5b far

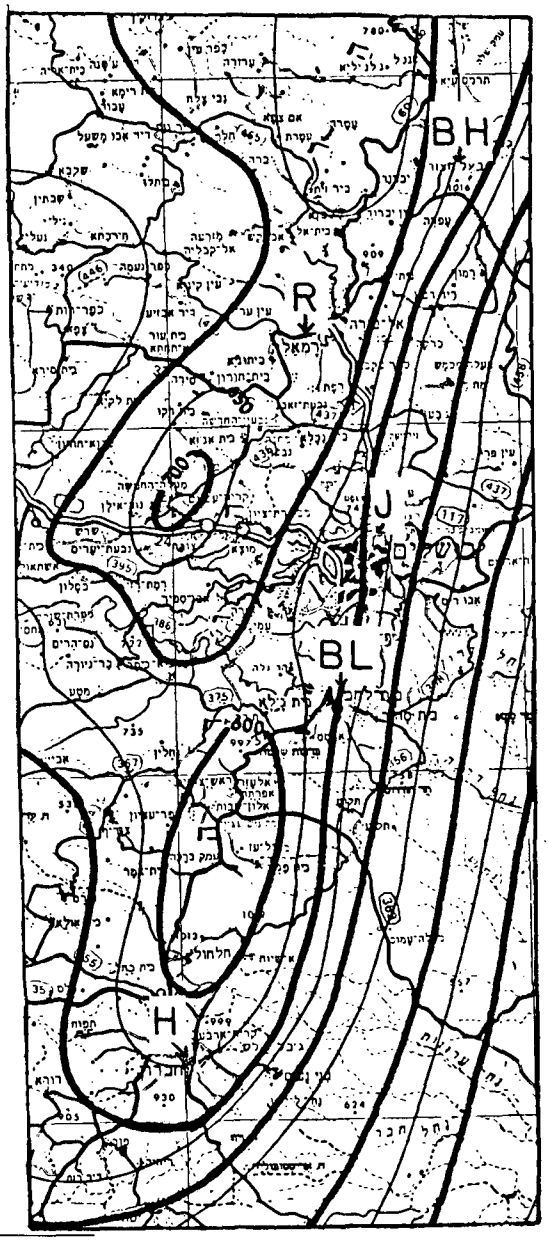

FIG. 2b. Observed contours of average annual rainfall based on data from about 58 gages (see Fig. 1b) during the period from 1951 to 1980. Rectangle designates the pertinent region from Fig. 2a [from a map published by the IMS (Israel Meteorological Service)]; contour interval of 50 mm yr^{-1}.

TABLE 2. Model against observed or radar-derived rainfall correlation coefficients. Numbers in parentheses stand for number of points for the pertinent correlation.

Experiment	Rural observations	All observations	Radar-derived precipitation
1. Annual	0.76*,† (41)	0.74*,† (56)	Annual rainfall normals from radar are not available
2. 18 Feb 1983	0.70* (23)	0.62* (29)	0.69* (276)
3. 31 Dec 1982–2 Jan 1983	0.45* (26)	0.38** (32)	0.51* (276)
4. 4 Mar 1983	0.80* (25)	0.56* (31)	0.71* (276)

* Significant at 1%.
** Significant at 5%.
† Two suspicious rainfall reports (Brechot–Shlomo, Arza) were excluded.

to the west of BL and adjacent to the big clutter area. This further strengthens our earlier point in section 4 that the model might be usefully employed to fill in gaps in the rainfall data. This is of particular importance in the mesoγ scale ($\Delta x \sim 2$ km) over complex topography where horizontal variability in rainfall could be considerably large.

Actually, one can nearly trace each maximum and minimum (+ and −) from the model simulation in the radar-derived rainfall (compare Figs. 5a and 5b). They are found to be in such a proximity in both maps that the translation vector of the + and − from Fig. 5a as compared to Fig. 5b could be drawn for nearly all maximum and minimum points and they are shown on both sides of Fig. 5b at the pertinent latitudes.

The correlation coefficients between the modeled and raingage-observed rainfall were found to be 0.62 (or 0.70 when urban observations were excluded as discussed later). The correlation coefficient with the radar-derived rainfall—276 points—is 0.69, quite close to the value obtained by correlating with 23 rural observations. Both values were found significant at the 99% level. These values indicate that a significant portion of the observed rainfall distribution in the small mesoscale could be explained by the model.

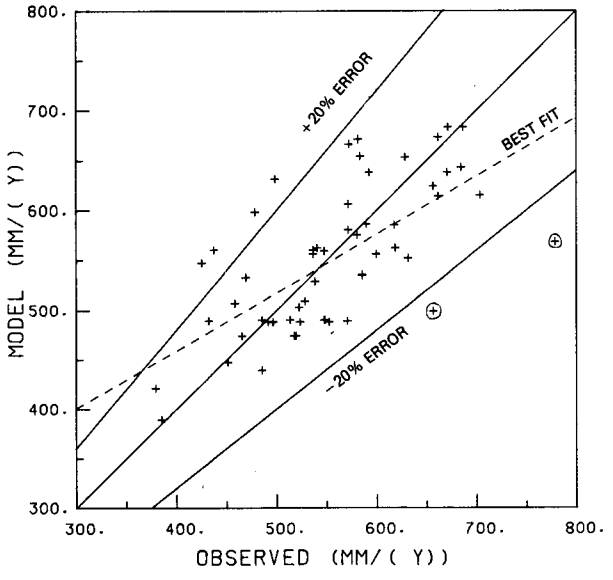

FIG. 3. Correlation between modeled and observed average annual rainfall, respectively. Best fit curve is given by $y = 0.59x \pm 225$ with correlation of 0.67. Lines with ±20% error are also drawn. Without the two circled points, correlation factor increases to 0.74.

A second case study was for the period of 31 December 1982–2 January 1983. The input parameters (Table 1) indicate that the wind direction is, as in the former case, directly from the west, though it is weaker. The larger integration period as well as the slightly higher sea surface temperature contributed to the higher rainfall values, but contrary to the case of 18 February the upstream rainfall values above the coast were also large ($P_0 = 50$ mm). The distribution (not shown) were similar to the 18 February case but the correlation coefficient is significantly lower—0.45 compared to 0.70 (Table 2). This low correlation for the December case is in agreement with Mishaeli's (1984) findings that the orographic contribution in the early winter is small. Mishaeli (1984) has performed a multivariable regressional analysis for rainfall data in Israel and has shown that the explained percentage of rainfall due to orography increased from 9 percent in December to 45 percent in March. The lesser role played by the orography in this case is also expressed in the lowest correlation coefficient between model and observed rainfall (see Table 2). But even in this case where orography did not play as major a role in determining the distribution of precipitation over the mountains, the resemblance in the rainfall patterns of the simulated and observed distributions was found to be high.

6. Simulated and radar-derived rainfall distributions—4 March 1983

Another late winter case occurred on 4 March 1983. The synoptic configuration is of a "Cyprus low" with cold air penetrating the eastern Mediterranean and becoming conditionally unstable over the relatively warm Mediterranean water. This configuration is similar to that described in section 5 for the 18 February case, and represents the typical system for most of the rainfall

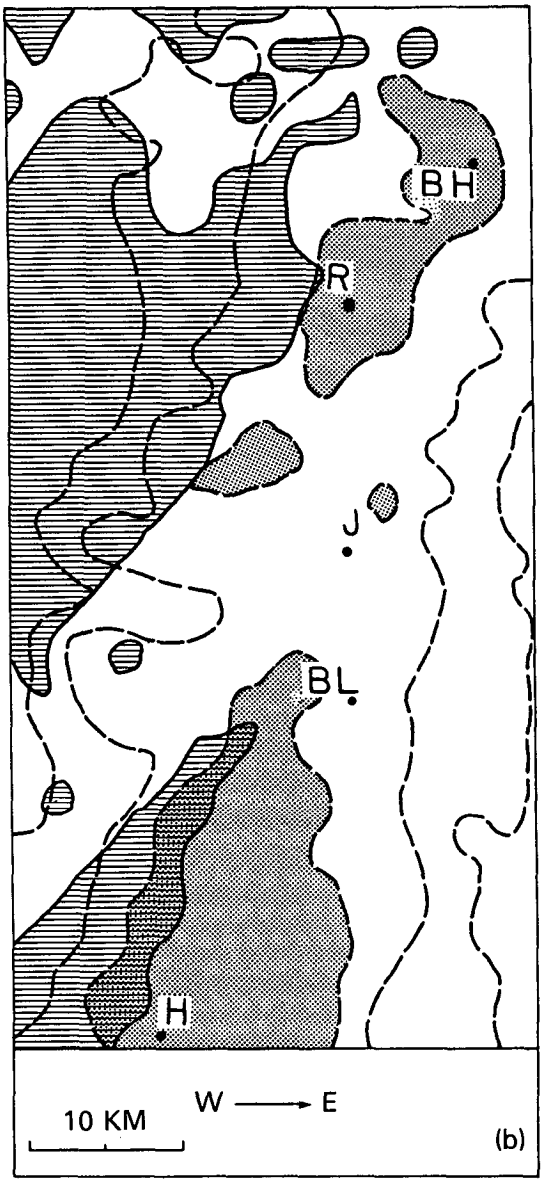

FIG. 4. Clutter regions in the simulated region. Horizontal hatching indicates the areas of permanent ground clutter. Points with only partial ground echo were also incorporated. Topographic contours as in Fig. 1b.

in the region; e.g., see Gagin and Neumann (1974). On 4 March 1983, however, the large-scale flow had also a significant southerly component, i.e., 240°/16.5 m s^{-1} compared to pure westerly winds in the former cases. Since the model is highly dependent on the wind vector component encountering the mountains, this case becomes important for testing the model ability to cope with changes in rainfall distributions induced by changes in wind direction. Moreover, relatively little is known about changes in rainfall distributions that are induced by changes in wind directions even though it was clearly shown, e.g., by Hill et al. (1981), that the wind vector plays the major role in orographic rain.

Figures 6a and 6b present the model and radar-derived rainfall for 4 March 1983. Input parameters (Table 1) are very close to those for 18 February 1983, except for the southwesterly wind direction. We first compare the radar-derived rainfalls on both cases, i.e., Figs. 6b and 5b, and then examine whether the model could cope with the observed differences. Comparison of the radar-derived distributions on Figs. 6b and 5b shows that the major features are similar. This is not a surprise as the change in wind direction is only by 30°. There are, however, a few significant differences as follows:

1) The rainfall trough from BH to the west here (4 March) is directly to the west (Fig. 6b) while on 18 February it is slightly rotated to the north (Fig. 5b). Compare the radar-derived rainfall values on the trough: (22, 22, 28) in Fig. 6b, and (12, 14, 16) in Fig. 5b.

2) The rainfall trough from Jerusalem (J) to the west-northwest splits close to the clutter domain on 4 March but not on 18 February; compare Figs. 6b and 5b.

3) The rainfall trough towards the north in the extreme northeastern boundary is clearly at a distance of one grid point west to the boundary (Fig. 6b), while on 18 February the trough is located on the boundary consisting of the values (6, 10, 14, 14).

4) The slope of the isohyets towards the east on 4 March (Fig. 6b) is stronger. This is clearly noticed in the south.

5) The rainfall ridge at the northeast corner of the southern clutter on 4 March extends farther to the north, i.e., to point (703, 508).

6) There are indications for additional maximum points on 4 March at approximately the locations (690, 540) and (700, 545).

When comparing the predictions for the two cases, i.e., Figs. 6a and 5a, *all* these differences between the two cases could also be traced in the model distributions even though the simulated structures are not as smooth, particularly on 4 March (Fig. 6a). For instance, the trough from BH westward is rotated to the north, as in the radar, for the 18 February case (Fig. 5a), but clearly directed to the west on 4 March simulation (Fig. 6a). The other differences in the observed distributions as well as some others, which are not mentioned, could be more or less traced in the simulations. A noticeable change between the two simulations is the different orientation of the rainfall patterns particularly west to J and BL. On 4 March with the southwesterlies prevailing the southwest–northeast orientation dominates (Fig. 6a), while on 18 February with the westerlies, the more east-to-west orientation dominates. In that sense the model overestimates the observed change as re-

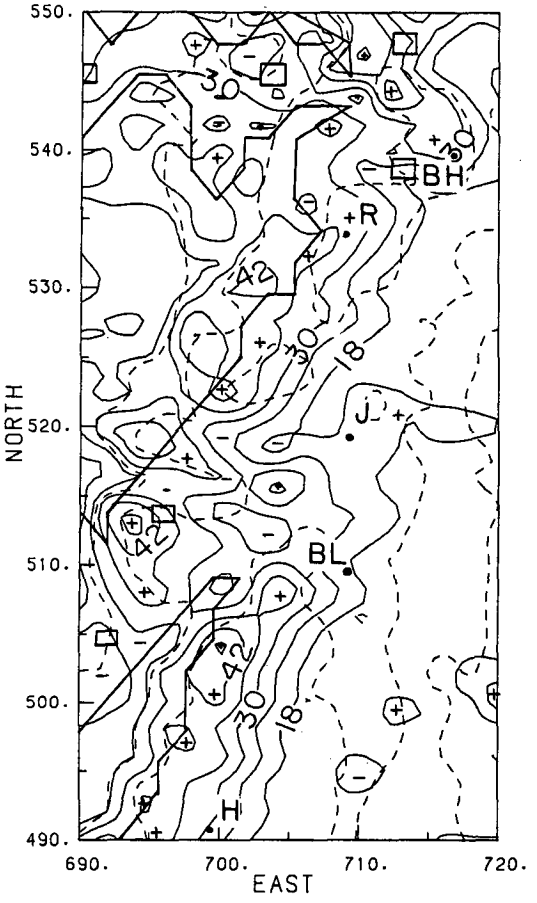

FIG. 5a. Model contours of total rainfall for 24 h starting at 0600 UTC 18 February 1982. Contour interval of 6 mm day^{-1}. Dashed lines are topographic contours as in Fig. 1b. The clutter areas from Fig. 4a are closed by heavy full lines. Maxima and minima as well as ridges and troughs in rainfall are indicated by + and −, respectively.

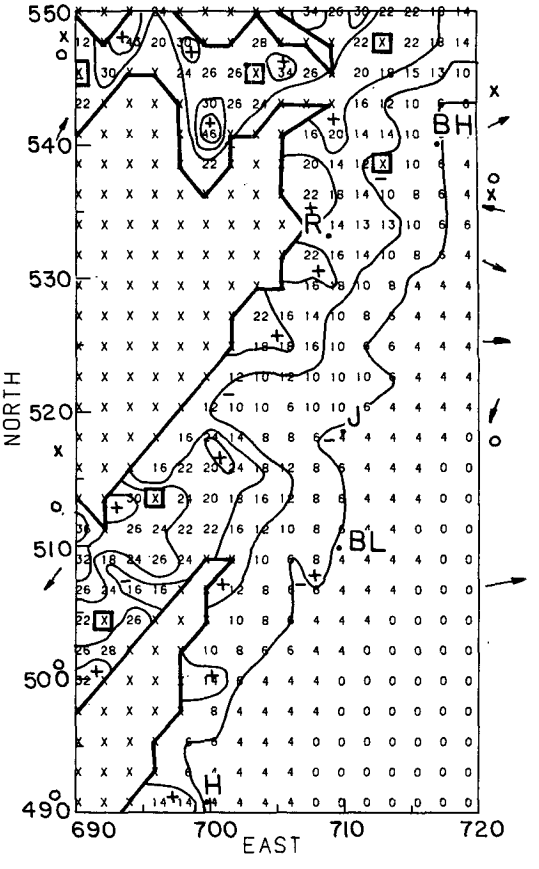

FIG. 5b. Observed contours of integrated rainfall for 24 h starting at 0600 UTC 18 February 1982 as derived from the radar measurements by Rosenfeld (1986). Gridded values in mm day^{-1} are indicated. Contour interval, clutter and + or − are as in Panel (a). Translation vectors of the location of the extremum points between model and observations are depicted on both sides at the pertinent latitudes. Circle denotes zero translation, while × denotes a disagreement.

flected in the radar-derived distributions. The reason for this overestimation lies probably in the focus of this model on the topographical effect ignoring other important physical processes like diffusion, which certainly smooths the orographic effect.

The major role played by the orography in the present case is also illustrated in the highest correlation coefficients obtained both in comparison with raingage measurements (0.80, when city reports were excluded) and the correlation with radar-derived rainfall (0.71). Both correlations are also highly significant in the statistical *t*-tests; see Table 2.

7. Discussion

a. Possible urban effect

The correlation between model and observed rainfall for 4 March is shown in Figs. 7a–c. In Figs. 7a and 7b the correlation is with raingage data with and without the city (Jerusalem) stations, respectively. It has been found that the six raingages in the city measured more rain than the out-of-city stations. On the average they collected 131 mm with a standard deviation (SD) of 9 while the out-of-city stations got 111 mm with SD = 20. The corresponding average values in the model are 104 (SD = 13) and 117 (SD = 21). These results were obtained although the average height of the city stations was slightly lower—758 meters, compared to 769 meters in the rural stations. The excess of rainfall in the city was typical for the other cases investigated here as well, and it was therefore suspected to be the result of an urban effect.[3] Since the urban effects are not parameterized by the model, we have also calculated correlation coefficients where the city stations were excluded. Consequently, the correlation coefficients have in-

[3] The possible urban effect is a matter of a separate study now being conducted by the authors. The study seems to indicate that the heat island and increased condensation nuclei effects are more important in Jerusalem compared to those of the roughness changes and the loss of evapotranspiration, see Shafir and Alpert (1989).

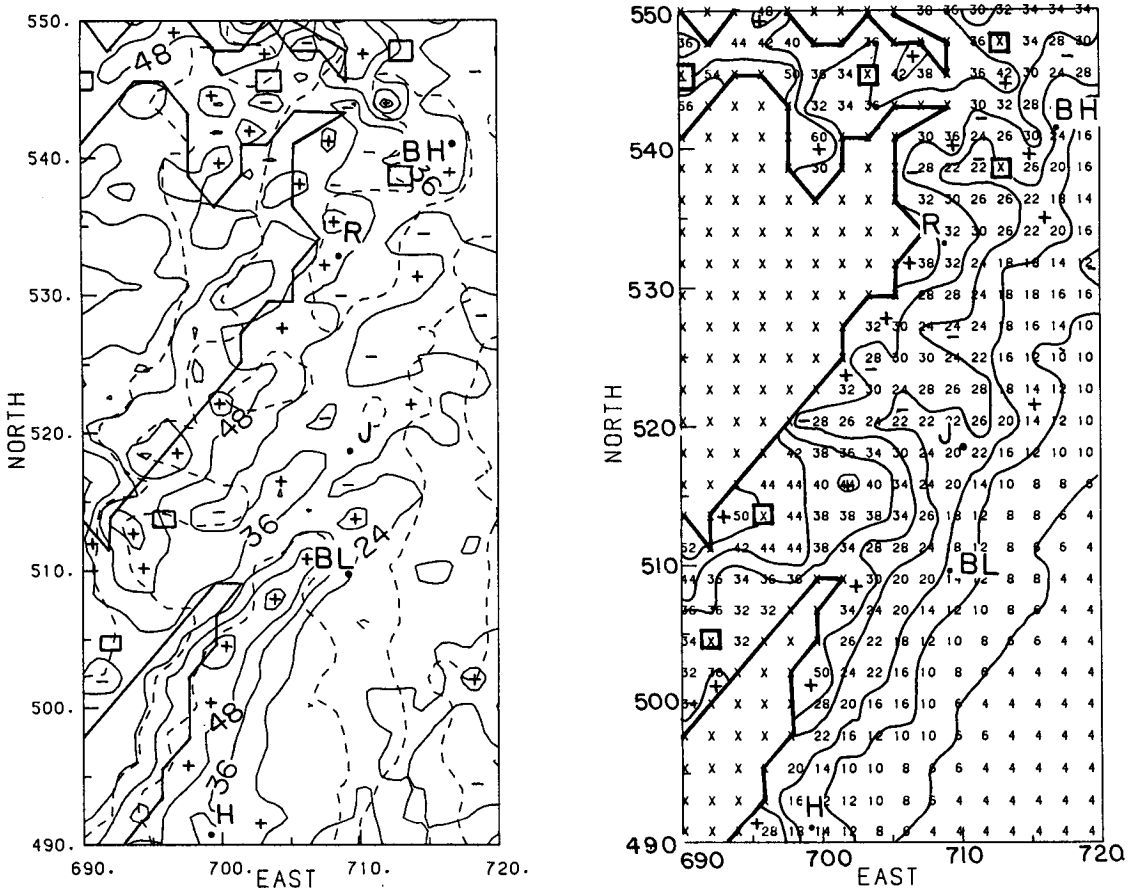

FIG. 6. (a) As in Fig. 5a but for 4 March 1983, and with a double contour interval of 12 mm day^{-1}.
(b) As in Fig. 5b but for 4 March 1983.

creased when the urban stations were excluded; see Table 2.

b. *Correlations between observed and simulated values*

Figure 7c presents the correlation of the model with radar-derived rainfall based on 276 data points (compare to Fig. 7b). The correlation coefficients of 0.71 or 0.80, with raingage data significant at 99%, indicate the model's ability to simulate certain features of the rainfall distribution. However, the best-fit lines in Figs. 7a–c are all with lower slopes, which shows that the model is worse in the extreme values. High rainfall values are underestimated while low rainfall values are overestimated by the model.[4] Such a model character could indicate that the smoothing is too strong, but it could also be caused by physical processes which were not incorporated into the model—for instance, any process that has horizontal variations of the flow, any relevant microphysical effects, any other cloud processes, or effects of stratification on the vertical velocity. Dynamical instabilities as well as the other processes could strongly influence the horizontal distribution of the rainfall. The lee-wave is an example of a phenomenon that could redistribute precipitation so that it will increase the rainfall in some places and decrease it in others.

c. *Sensitivity studies*

One of the important questions regarding any model is related to the model sensitivity to variations in the input parameters. Table 3 lists a series of experiments in which the annual run was repeated but in each case with a change in only one of the model parameters by a realistic increment representing a hypothetical change in the relevant input parameter. In addition to the average and maximum differences percentage-wise that were induced by the relevant change, the last row presents the standard deviation of the normalized differences. This is a convenient measure of the effect the respective change had on the rainfall distribution. Of course, the results depend to some extent on the specific topographical location of the points involved in the sensitivity study and on the basic experiment. We have

[4] A similar discrepancy was noticed also by Collier (1975, Fig. 6).

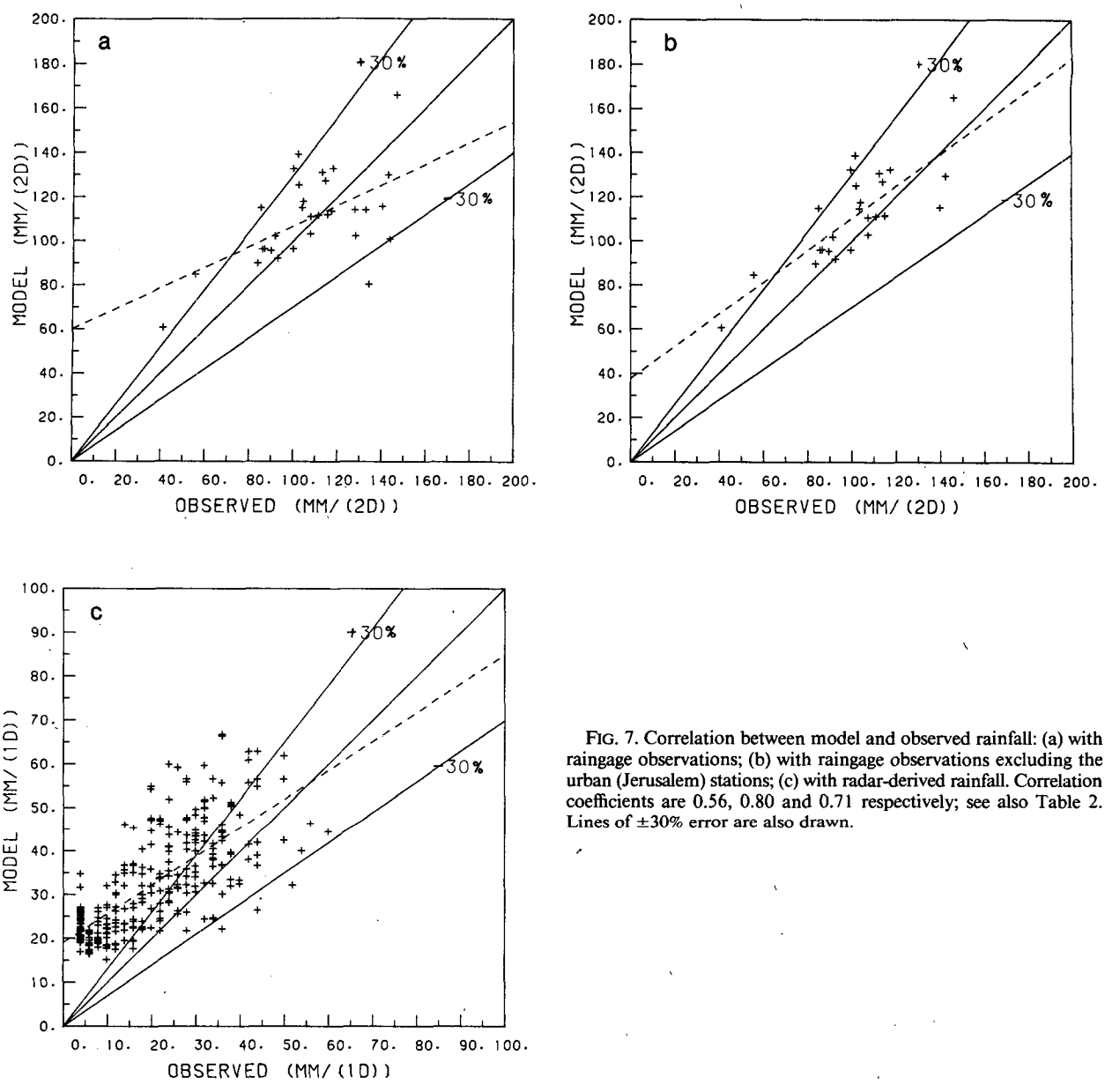

FIG. 7. Correlation between model and observed rainfall: (a) with raingage observations; (b) with raingage observations excluding the urban (Jerusalem) stations; (c) with radar-derived rainfall. Correlation coefficients are 0.56, 0.80 and 0.71 respectively; see also Table 2. Lines of ±30% error are also drawn.

therefore chosen 12 representative points in the area as follows: 4 equidistant points on each of three longitudes crossing the model domain. The sensitivity study results clearly indicate that wind direction and RH (relative humidity) upstream are the most sensitive model parameters. Although the maximum difference is also large for an increase in upstream precipitation (27.2%), the influence on the SD (standard deviation) of the normalized differences is small (±3.0%). The latter indicates a relatively small change in the distribution. Obviously, these changes are only reflected in the percentage-wise representation, since the absolute orographic contributions are independent of the upstream precipitation in the present model formulation. The next two sensitive parameters are the topographic altitude and the horizontal resolution. Both are associated with an SD value for the normalized differences which exceeds 7 percent; see Table 3. It should be mentioned that change of topographic altitude is equivalent to a change of slope.

d. Other models for orographic rain

Another question of interest is the comparison of the present model with other orographic rainfall models. These models could be divided into two major

TABLE 3. Sensitivity tests for the model parameters. The basis for the tests was the annual run and 12 representative points (4 equidistant points on each of three longitudes crossing the domain).

Parameter	Value in annual experiment	Increment	Average of difference (%)	Maximum differences (%)	Standard deviation of the normalized differences (%)
Wind direction (deg)	270	+30	+3.9	+18.4	±5.9
		−30	+0.7	−6.5	±3.7
		+90	−2.3	+16.6	±10.5
		−90	−8.6	−29.3	±14.7
Wind speed (m s^{-1})	10	±5	±8.9	±16.6	±5.6
Topographic altitude	Given height	double	+10.8	+18.4	±7.1
		half	−7.8	−14.3	±4.9
RH at MSL (%) (northwest corner)	100	−20	−3.5	−6.6	±2.2
		−40	−7.1	−13.3	±4.5
RH variation (%) upstream (x-east)	−15	±15	∓8.8	∓16.4	±5.8
RH variation (%) upstream (y-north)	+30	±30	∓19.0	∓34.6	±11.7
MSL temperature (K)		+5	+6.2	+11.6	±3.9
	291	−5	−4.7	−8.9	±3.0
Lapse-rate (K km^{-1})	−6.5	+2.5	+1.6	+3.5	±1.2
		−2.5	−1.4	−3.2	±1.1
Rain period (days)	47	+23.5	+8.5	+15.9	±5.3
		−23.5	−9.0	−16.8	±5.6
Upstream precipitation (mm)	550	±150	±22.4	±27.2	±3.0
Advection parameter σ (km)	4	+4	−0.4	−7.1	±3.7
		−2	+0.1	+11.5	±6.0
Δx (km)	2	+2	+1.1	+13.1	±6.3
		−1	+0.9	+11.6	±7.7

groups: 1) the dynamical models that start with some physical considerations and 2) the statistical models. Rhea (1978) has presented a simplified dynamical model for orographic rain and has obtained high correlation coefficients—0.75 to 0.94—for seasonally summed averages over western Colorado. Rhea indicates, however, that for short periods such as 6 to 24 hours, correlation coefficients drop to 0.70–0.80. These values are certainly within the range of the present model (see Table 2), although our model does not solve explicitly a parcel-following water budget equation as was proposed by Rhea. Although Rhea showed the importance of the moisture depletion by upstream barriers, it was not explicitly calculated here because its effect on a relatively much smaller region (30 km total width in the present study) was assumed less important. Also, this effect was partly accounted for by inputting the model with an east-to-west (across the barrier) relative humidity variation (Table 1). Another significant difference is our focus on a finer scale, horizontal resolution of 2 km compared with 10 km in Rhea. Also, quantitative comparison with radar-derived rainfall at these small scales is of special interest in the present study and, to the best of our knowledge, is done here for the first time.

Similar studies of orographic rainfall for forecasting purposes were conducted by Collier (1975) and Bell (1978). The major difference is the comparison done in the present study at a 2-km scale while these other studies focused on much larger scales. As indicated by Collier (1975, p. 411), who introduced additional contributions to the vertical velocity, in all cases, the dominant term was the term we used, i.e., $\mathbf{V} \cdot \nabla Z_s$. Collier found a mean error in the predicted rainfall of ±10% over 10^3 km^2 and of ±20% over 10^2 km^2. In the present study we found a mean error of ±8.4% for the mean annual normals and ±15 to 20% for the three case studies. It is therefore suggested that the orographic rainfall at the smaller (finer) mesoscale (ΔX = 2 km) becomes even more predictable than the larger mesoscale (ΔX = 10 km). The relatively higher predictability on the smaller scales is particularly noticeable for climatological averages. The reason for this could be the dominant effect of the mechanical uplifting by orography at the smaller mesoscale with a horizontal grid of 2 km.

Statistical methods for orographic rain have been applied successfully with sometimes very high correlation coefficients in many regions and also in Israel (e.g., see Wolfson 1975; Mishaeli 1984). However, these

methods work well mainly for long-range averages such as standard normals and where a relatively large number of observations is available. Consequently, these methods are not appropriate for sparse-data regions or for case studies as done in the present study.

e. Rainfall efficiencies

The rainfall efficiency served in the present study as a tuning parameter to bring the *average* model precipitation to that which was observed. The annual value of 0.1 (Table 1) was found the lowest, probably because the 47 annual-averaged number of rainfall days consists of days in which the precipitation occurred only during a small fraction of the day (a minimum diurnal amount of 1 mm). In contrast, the periods for the three cases chosen, were, more or less, periods of continuous rain. The resulting efficiency factors for the three cases increase towards the end of the winter period of rain. From a value of 0.33 in December it increases to 0.5 and 0.75 in February and March, respectively. As pointed out earlier this seems to be the result of the increased effect of topography at the end of the winter.

8. Conclusions

The advantages of applying relatively simple models as the one presented here are threefold. First, more sophisticated models could always be compared with such models to easily verify the possible advantage in the inclusion of further processes. Second, the model could be used in conjunction with statistical models to complement annual normals in data-free regions (see section 4). And last but not least, in the planning of raingage networks the model output could serve as an initial guide for regions of high and low gradients of precipitation (section 5, 6).

The evidence presented in this paper supports the idea that mesoγ-scale distributions of orographic precipitation are primarily a direct result of linear orographic uplifting due to the horizontal wind vector encountering mountain slopes. In particular, predicted distributions of precipitation over the Judean Mountains, Israel, are compared to observed distributions as derived from radar measurements for a few specific cases as well as to averaged annual rainfall based on the raingage network. It was shown that the model accounts for many of the averaged mesoscale features of rainfall distribution with a horizontal grid interval of 2 km. Following our results at the mesoγ-scale and Rhea's (1978) results on the mesoβ-scale it seems that one of the more basic findings of this study is that the mesoγ-scale orographic precipitation with the adiabatic uplift assumptions is at least as highly predictable as for the mesoβ-scale, if not higher.

It should be emphasized that the usefulness of quantitative radar precipitation measurements is doubtful because the error in the amount of precipitation obtained in this way might be very large. But, following several studies it seems that radar-derived precipitation could be successfully applied for studying the patterns of the orographic precipitation.

The mean error in the predicted rainfall on a scale of 2 km was found to be as low as $\pm 8.4\%$ for mean annual normals and 15%–20% for the three case studies, which for the first time illustrates the relatively high rainfall predictability in the small mesoscale.

It was illustrated that the climatological observed rainfall distribution could be effectively complemented by the model at locations where sufficient observations were unavailable. A detailed discussion of the method for complementing rainfall distributions over the Judean and Galilee mountains, Israel, is described by Alpert and Shafir (1988).

The high sensitivity of the orographic rain to the horizontal wind speed as found here and as indicated by Browning (1980) and Richard et al. (1987) suggests that further research should take the following directions:

1) Include more sophisticated relations for the vertical velocities above the mountain, for example, nonlinear models that calculate the mountain wave dynamics.

2) In regions where sufficient rainfall data is available, the conjunction of both statistical models and simple dynamical models might yield the best estimations for rainfall rates over complex terrain.

Acknowledgments. We wish to thank the Israel Meteorological Service and Dr. D. Rosenfeld for supplying the data. Thanks for useful comments go also to Profs. D. Atlas and R. Pielke. We also acknowledge the help by J. Mishaeli and D. Decker. We thank Ms. Rachel Duani for typing the manuscript and Mr. A. Dvir for preparing the figures.

REFERENCES

Alpert, P., 1986: Mesoscale indexing of the distribution of orographic precipitation over high mountains. *J. Climate Appl. Meteor.*, **25**, 532–545.

——, and H. Shafir, 1989: A physical model to complement rainfall normals over complex terrain. *J. Hydrol.*, in press.

Bader, M. J., and W. T. Roach, 1977: Orographic rainfall in warm sectors of depressions. *Quart. J. Roy. Meteor. Soc.*, **103**, 269–280.

Bell, R. S., 1978: The forecasting of orographically enhanced rainfall accumulations using 10-level model data. *Meteor. Mag.*, **107**, 113–124.

Bergeron, T., 1965: On the low-level redistribution of atmospheric water caused by orography. *Supp. Proc. Int. Conf. Cloud Phys.*, IAMAP/WMO Tokyo, 96–100.

Browning, K. A., 1980: Structure, mechanism and prediction of orographically enhanced rain in Britain. *Orographic Effects in Planetary Flows*, R. Hide and P. W. White, Eds., GARP Publ. Ser. No. 23, 85–114.

Collier, C. G., 1975: A representation of the effects of topography on surface rainfall within moving baroclinic disturbances. *Quart. J. Roy. Meteor. Soc.*, **101**, 407–422.

——, and J. M. Knowles, 1986: Accuracy of rainfall estimates by radar. Part III: Application for short-term flood forecasting. *J. Hydrol.*, **83**, 237–249.

Gagin, A., and J. Neumann, 1974: Rain stimulation and cloud physics in Israel. *Weather and Climate Modification*, W. N. Hess, Ed., Wiley and Sons, 454–494.

Hill, F. F., K. A. Browning and M. J. Bader, 1981: Radar and rain-gauge observations of orographic rain over south Wales. *Quart. J. Roy. Meteor. Soc.*, **107**, 643–670.

Holton, J. R. 1979: *An Introduction to Dynamic Meteorology*, 2nd ed., Academic Press, 391 pp.

Mishaeli, J., 1984: The geographic influences on rainfall in Israel. *Meteorologia B'Israel.* **84-2.**

Rhea, J. O., 1978: Orographic precipitation model for hydrometeorological use. Ph.D. thesis, Colorado State University, Atmos. Sci. Paper No. 287, 198 pp.

Richard, E., N. Chaumerliac, J. F. Mahfouf and E. C. Nickerson, 1987: Numerical simulation of orographic enhancement of rain with a mesoscale model. *J. Climate Appl. Meteor.*, **26**, 661–669.

Rosenfeld, D., 1986: Dynamic characteristics of cumuliform cloud and cloud systems, and their effect on the rainfall precipitated by them. Ph.D. thesis, The Hebrew University of Jerusalem, 143 pp.

Shafir, H., and P. Alpert, 1989: On the urban rainfall anomaly in Jerusalem—a numerical study. *Atmos. Environ.*, submitted.

Stevens, D. E., and R. S. Lindzen, 1978: Tropical wave–CISK with a moisture budget and cumulus friction. *J. Atmos. Sci.*, **35**, 940–961.

Storebo, P. B., 1976: Small scale topographic influences on precipitation. *Tellus*, **28**, 45–49.

Wolfson, N., 1975: Topographical effects on standard normals of rainfall over Israel. *Weather*, **3**, 138–144.